

Explainability in Generative Medical Diffusion Models: A Faithfulness-Based Analysis on MRI Synthesis

Surjo Dey and Pallabi Saikia *

Rajiv Gandhi institute of petroleum technology, Amethi, Uttar Pradesh, India
 22cs3072@rgipt.ac.in, psaikia@rgipt.ac.in

Abstract. This study investigates the explainability of generative diffusion models in the context of medical imaging, focusing on Magnetic resonance imaging (MRI) synthesis. Although diffusion models have shown strong performance in generating realistic medical images, their internal decision making process remains largely opaque. We present a faithfulness-based explainability framework that analyzes how prototype-based explainability methods like ProtoPNet (PPNet), Enhanced ProtoPNet (EPP-Net), and ProtoPool can link the relationship between generated and training features. Our study focuses on understanding the reasoning behind image formation through denoising trajectory of diffusion model and subsequently prototype explainability with faithfulness analysis. Experimental analysis shows that EPPNet achieves the highest faithfulness (with score 0.1534), offering more reliable insights, and explainability into the generative process. The results highlight that diffusion models can be made more transparent and trustworthy through faithfulness-based explanations, contributing to safer and more interpretable applications of generative AI in healthcare.

Keywords: Explainability, Medical Image synthesis, Diffusion model, MRI, Prototype Learning

1 Introduction

Diffusion based generative models have recently become a leading approach for generating high-quality synthetic images. These models learn to reverse a gradual noise adding process, turning random noise into realistic images step by step [7] [19]. Compared with earlier approaches such as GANs [5] or VAEs [13], diffusion models are more stable during training and have a solid mathematical foundation, which makes them promising for sensitive applications like medical imaging [12]. However, two major challenges still limit their broader use in healthcare. The first is the lack of strong convergence guarantees when working with complex and noisy medical data. The second, and more critical, is the limited explainability of these models. It is often unclear how the generated images

*Corresponding author

relate to the training data or what influences specific visual features during the generation process. This lack of transparency reduces trust and makes it difficult to apply such models in clinical settings.

Recent studies have begun exploring the integration of explainability mechanisms into diffusion-based generative models for medical imaging. Recent works, including VALD-MD (2024) [17] and Latent Diffusion Attribution (2024) [18] employs latent diffusion to reconstruct normal counterparts of abnormal scans, providing voxel-level attributions for diagnostic insight. While The Mediffusion framework (2024) [11] jointly trains diffusion and classification objectives to achieve self-explainable semi-supervised generation. Unlike prior multi-class attribution studies, we propose a prototype-based faithfulness framework for single-class medical diffusion that directly associates generated features with their real training origins. These advances demonstrate a growing trend toward faithful and interpretable diffusion frameworks in healthcare, motivating the present study's prototype-based faithfulness analysis for explainable MRI synthesis. Although explainability has been widely explored in classification or diagnostic models, it has received far less attention in generative systems. In particular, understanding how diffusion models create new medical images, such as MRI scans still remains an open question [2].

This work investigates the prototype-based explainability for generative diffusion models that synthesize breast MRI images for segmentation. Our key contributions include:

- We proposed a faithfulness-based explainability framework that integrates prototype-based reasoning with diffusion-based medical image generation model.
- We analyzed three prototype-based explainability models (PPNet, EPP-Net, ProtoPool) to systematically quantify the interpretability of diffusion-generated MRI images.
- The models are evaluated on different Image quality analysis metrics PSNR, SSIM, LPIPS to analyse the visual quality of diffusion synthesised images and Faithfulness Score metric is applied for analysing the alignment of prototype activations with generative dynamics.
- The experiments are performed on the publicly available medical imaging dataset, the DUKE Breast MRI data set, demonstrating the reasoning for realistic synthesis of MRI data using diffusion model with explainable generation trajectories and faithfulness scores.

While many existing studies depends on multiple classes, our task involves only one single anatomical class, focusing purely on image level relationships. We evaluate how different prototype-based explainability methods can trace the influence of real training examples on generated images. Our analysis shows that prototype-based reasoning can provide faithful and interpretable explanations even in single class medical domains [3] [10]. By linking the generative process with meaningful explanations, we take a step toward more transparent and trustworthy AI for medical imaging.

2 Methodology

This research explores the explainability of diffusion based generative models applied to breast MRI synthesis. The methodology combine a diffusion model architecture for generating realistic MRI images with prototype based neural networks that provide interpretable mappings between generated and real data samples. The objective is to explore whether these models can offer faithful explanations of how specific image features emerge during the generative process. Our approach focuses on a single class medical imaging domain, where all data belong to the same anatomical category, ensuring that variations appear only from structural or textural differences rather than semantic class distinctions. By combining the stochastic generative dynamics of diffusion models with prototype learning, we aim to construct a framework that not only synthesizes anatomically accurate MRI images but also reveals which regions or training examples most influence the generated outputs.

2.1 Diffusion Model Architecture for MRI Synthesis

Diffusion models are generative frameworks that learn to reverse a gradual noising process, transforming random noise into structured images. In our context, the model is trained to generate realistic breast MRI images by progressively denoising a sample from a Gaussian distribution using Denoising Diffusion Probabilistic Models [7]. The learning objective is to approximate the reverse of a fixed forward diffusion process that slowly adds noise to real MRI data.

The forward diffusion process can be expressed as a Markov chain that adds Gaussian noise to an image x_0 over T time steps. Each step produces a slightly noisier version x_t according to:

$$q(x_t|x_{t-1}) = \mathcal{N}(x_t; \sqrt{1 - \beta_t} x_{t-1}, \beta_t \mathbf{I}), \quad (1)$$

where β_t represents the variance schedule controlling the noise level at step t . This process gradually destroys image information until x_T becomes nearly pure noise.

To generate new samples, the model learns a reverse process parameterized by θ :

$$p_\theta(x_{t-1}|x_t) = \mathcal{N}(x_{t-1}; \mu_\theta(x_t, t), \Sigma_\theta(x_t, t)), \quad (2)$$

where μ_θ and Σ_θ are predicted by a neural network, typically a U-Net or its variant. This network learns to estimate either the mean of the clean image or the noise added during the forward process.

Training aims to minimize the difference between the true noise ϵ added during diffusion and the model's predicted noise $\epsilon_\theta(x_t, t)$:

$$\mathcal{L}_{\text{simple}} = \mathbb{E}_{x_0, \epsilon, t} [\|\epsilon - \epsilon_\theta(x_t, t)\|^2]. \quad (3)$$

This loss encourages the model to denoise accurately at each time step, effectively learning how to reconstruct realistic MRI images from noise. During inference,

the model iteratively applies the learned reverse process, gradually converting random noise into a coherent breast MRI image.

To further improve anatomical consistency, the diffusion process is conditioned on additional information such as segmentation maps or structural priors [8], [14], [4]. In this setup, the model learns a conditional distribution $p_\theta(x_{t-1}|x_t, y)$, where y encodes prior knowledge about tissue boundaries or organ structure. This conditioning allows the generated MRI images to better preserve spatial alignment and realistic anatomical details.

2.2 Prototype-Based Explainability Framework

To make the generative diffusion model explainable, we employ a prototype-based framework that links generated MRI images to representative training samples. Prototype learning assumes that each model decision can be explained through a small set of learned image regions, called prototypes, which represent typical local patterns observed in the data [3]. When the model generates a new image, it can be interpreted as a combination of these prototypes, allowing us to trace how specific visual features emerge.

Prototype-based models differ from standard convolutional neural networks by including an additional layer that explicitly stores a set of prototype vectors $\{p_j\}_{j=1}^m$ in the latent feature space. These prototypes are compared with local feature patches extracted from an image through similarity measures such as the squared Euclidean distance. Given a feature map $f(x) \in \mathbb{R}^{H \times W \times D}$, the similarity between a feature patch $f(x)_{hw}$ and a prototype p_j is computed as:

$$s_{j,hw} = -\|f(x)_{hw} - p_j\|_2^2, \quad (4)$$

where higher similarity indicates that the local region resembles the prototype. The model then aggregates these similarities to form interpretable predictions or associations.

In our study, we explore three main prototype-based architectures: ProtoPNet (PPNet) [3], Enhanced ProtoPNet (EPPNet) [1], and ProtoPool [15]. Each provides a different mechanism for learning and updating prototypes, thereby offering distinct interpretability properties Figure 1.

ProtoPNet (PPNet) The Prototype Propagation Network (ProtoPNet) forms the foundation of prototype-based explainability. It introduces an interpretable layer that associates learned prototypes with specific regions in an image. Each prototype represents a feature patch extracted from the training set and acts as an example of a visual concept, such as a texture or structure within an MRI scan.

The model architecture typically follows a convolutional backbone (e.g., ResNet or U-Net encoder) followed by a prototype layer and a fully connected classification head. The output of the prototype layer is a similarity score between each prototype p_j and the input feature map $f(x)$, computed as:

$$g_j(x) = \max_{h,w} s_{j,hw} = -\min_{h,w} \|f(x)_{hw} - p_j\|_2^2, \quad (5)$$

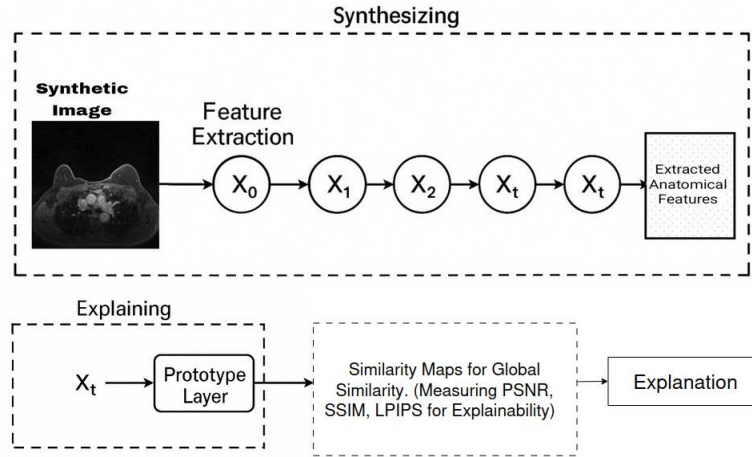


Fig. 1: Overall architecture of the proposed diffusion based explainability framework. The process begins with prototype based interpretation of extracted anatomical features. The learned prototypes identify feature level correspondences between synthetic and real MRI regions, providing an interpretable understanding of the generative process.

where $s_{j,hw}$ represents the similarity between the prototype and the feature at position (h, w) . This allows each prototype to focus on the most relevant image region.

Training involves two objectives: classification accuracy and prototype alignment. The alignment loss encourages prototypes to remain close to the feature patches they represent:

$$\mathcal{L}_{\text{align}} = \sum_j \min_{x \in X_j} \|p_j - f(x)_{h^*, w^*}\|_2^2, \quad (6)$$

where X_j denotes the set of samples associated with prototype p_j . This mechanism ensures that prototypes correspond to real, meaningful regions from the training images, improving interpretability.

Enhanced ProtoPNet (EPPNet) The Enhanced ProtoPNet (EPPNet) builds upon the original PPNet by introducing additional mechanisms for prototype normalization and interpretability scoring. EPPNet refines prototype learning through a normalization process that stabilizes similarity scores across prototypes and improves faithfulness in explaining generated data.

The key idea is to compute normalized influence scores that quantify how strongly each prototype contributes to an image. The normalized influence of prototype p_j for image x is defined as:

$$NIS_j(x) = \frac{\exp(g_j(x))}{\sum_{k=1}^m \exp(g_k(x))}, \quad (7)$$

where $g_j(x)$ is the similarity activation from the prototype layer. This normalization converts similarity scores into probabilities, allowing the model to measure the contribution of each prototype to the overall representation.

EPPNet also introduces a regularization term that ensures prototypes remain diverse and capture different regions or structures:

$$\mathcal{L}_{\text{div}} = \sum_{i \neq j} \exp(-\|p_i - p_j\|_2^2). \quad (8)$$

This diversity loss prevents prototypes from collapsing into similar patterns, thereby improving both visual coverage and interpretability. In practice, EPPNet provides more faithful explanations by highlighting which prototypes most influence a generated MRI image, linking synthetic features to their corresponding real patterns in the dataset.

ProtoPool ProtoPool extends the prototype-based framework by introducing a dynamic pooling mechanism that allows prototypes to be shared or merged across related samples. Unlike PPNet and EPPNet, which maintain fixed prototype assignments, ProtoPool organizes prototypes into a shared latent pool that can adaptively allocate prototypes based on feature similarity.

Let $\mathcal{P} = \{p_1, p_2, \dots, p_m\}$ denote the prototype pool, and let α_{ij} represent the assignment weight between feature $f(x)_i$ and prototype p_j . The pooled representation is computed as:

$$z_i = \sum_{j=1}^m \alpha_{ij} p_j, \quad \text{where} \quad \alpha_{ij} = \frac{\exp(-\|f(x)_i - p_j\|_2^2)}{\sum_{k=1}^m \exp(-\|f(x)_i - p_k\|_2^2)}. \quad (9)$$

This formulation allows multiple prototypes to contribute jointly to each image region, capturing finer-grained patterns that may appear in medical data.

ProtoPool improves flexibility by letting the model reuse prototypes for related structures, such as similar tissue textures across different MRI slices. This pooling-based design helps maintain interpretability while providing a richer representation of complex anatomical variations. However, since prototypes are no longer strictly tied to a single image patch, ProtoPool explanations may be less localized compared to PPNet or EPPNet but offer greater generalization capacity.

2.3 Faithfulness Evaluation Metrics

To assess the interpretability and reliability of generated MRI images, we employ a set of quantitative metrics that evaluate both perceptual quality and faithfulness to the original training data. The selected measures include Peak Signal-to-Noise Ratio (PSNR) [9], Structural Similarity Index (SSIM) [20], Learned Perceptual Image Patch Similarity (LPIPS) [21], and a Faithfulness Score derived from prototype-based influence estimation. Together, these metrics provide a comprehensive evaluation of image reconstruction quality and the extent to which generated images preserve meaningful relationships with their source data.

Peak Signal to Noise Ratio (PSNR) Peak Signal-to-Noise Ratio is a classical metric used to measure the fidelity between a generated image \hat{x} and its ground-truth counterpart x . It quantifies the amount of reconstruction error in terms of pixel-wise differences. The mean squared error (MSE) between two images is defined as:

$$\text{MSE} = \frac{1}{N} \sum_{i=1}^N (x_i - \hat{x}_i)^2, \quad (10)$$

where N is the total number of pixels. The PSNR value is then computed as:

$$\text{PSNR} = 10 \cdot \log_{10} \left(\frac{L^2}{\text{MSE}} \right), \quad (11)$$

where L denotes the maximum possible pixel intensity value (for normalized images, $L = 1$). A higher PSNR indicates smaller reconstruction errors and higher image fidelity. Although PSNR provides a simple and interpretable measure, it is sensitive to minor pixel variations and may not fully reflect perceptual quality.

Structural Similarity Index (SSIM) The Structural Similarity Index (SSIM) evaluates image quality based on structural consistency rather than absolute pixel differences. It measures the similarity between the luminance, contrast, and structure of two images, defined as:

$$\text{SSIM}(x, \hat{x}) = \frac{(2\mu_x\mu_{\hat{x}} + C_1)(2\sigma_{x\hat{x}} + C_2)}{(\mu_x^2 + \mu_{\hat{x}}^2 + C_1)(\sigma_x^2 + \sigma_{\hat{x}}^2 + C_2)}, \quad (12)$$

where μ_x and $\mu_{\hat{x}}$ are the mean intensities, σ_x^2 and $\sigma_{\hat{x}}^2$ are the variances, and $\sigma_{x\hat{x}}$ is the covariance between x and \hat{x} . Constants C_1 and C_2 stabilize the division against weak denominators. SSIM values range from 0 to 1, with 1 indicating perfect structural similarity. This metric aligns more closely with human visual perception and is particularly suitable for medical imaging where structural integrity is critical.

Learned Perceptual Image Patch Similarity (LPIPS) While PSNR and SSIM rely on pixel-wise or low-level features, the Learned Perceptual Image Patch Similarity (LPIPS) metric uses deep feature representations from pre-trained convolutional networks to estimate perceptual differences. Let $\phi_l(x)$ and $\phi_l(\hat{x})$ denote the activation maps extracted from layer l of a pretrained network (e.g., VGG or AlexNet). The LPIPS distance between x and \hat{x} is computed as:

$$\text{LPIPS}(x, \hat{x}) = \sum_l w_l \|\hat{\phi}_l(x) - \hat{\phi}_l(\hat{x})\|_2^2, \quad (13)$$

where $\hat{\phi}_l$ denotes normalized feature maps and w_l are learned weights that capture the relative importance of each layer. Lower LPIPS values indicate higher perceptual similarity. This metric captures subtle structural and textural differences that are often overlooked by traditional measures, making it highly relevant for assessing the realism of diffusion-generated MRI images.

Faithfulness Score Beyond visual quality, interpretability requires that model explanations accurately reflect the true generative process. The Faithfulness Score quantifies the consistency between the influence estimated by prototypes and the actual contribution of training examples to a generated image. It measures how well the prototype-based explanation aligns with the underlying diffusion generation dynamics.

Given a set of normalized influence scores $\{NIS_j(x)\}_{j=1}^m$ for a generated image x , where $NIS_j(x)$ represents the relative contribution of prototype p_j , the faithfulness score is defined as:

$$F(x) = \frac{1}{m} \sum_{j=1}^m NIS_j(x) \cdot \text{corr}(p_j, x), \quad (14)$$

where $\text{corr}(p_j, x)$ denotes the spatial correlation between prototype p_j and the corresponding region in x . The resulting score lies in $[0, 1]$, where higher values indicate more faithful and consistent explanations.

This metric provides an intrinsic measure of interpretability by linking the visual and statistical consistency of prototype activations with the diffusion process itself. In the context of medical imaging, a high faithfulness score implies that the model explanations reliably represent which anatomical patterns influenced the generation of synthetic MRI images, thereby strengthening the trustworthiness of the generative framework.

3 Results and Discussion

3.1 Dataset

The experiments in this study were conducted using the DUKE Breast MRI dataset [16], a well established collection of dynamic breast magnetic resonance images. This dataset contains a wide range of breast tissue appearances, lesion types, and anatomical variations, providing a robust foundation for evaluating generative models in medical imaging. From this dataset, a subset of high resolution scans (11860 MRI Images) was used to train a diffusion model designed for single class image synthesis. The diffusion model was trained in a supervised setting, conditioned on anatomical segmentation maps to preserve spatial coherence and enhance the realism of synthesized images.

After training, the model generated synthetic breast MRI images that were quantitatively evaluated against the original data distribution. The Frechet Inception Distance (FID) [6] was measured at 1.39, indicating that the generated samples were highly similar to real images in feature space. Additionally, the segmentation based Dice similarity coefficient achieved a value of 0.9478, confirming that anatomical structures were accurately reproduced in the synthesized outputs. These results suggest that the diffusion model effectively captured the fine-grained visual and structural characteristics of breast MRI images while maintaining high fidelity and anatomical consistency, as shown in Figure 2.

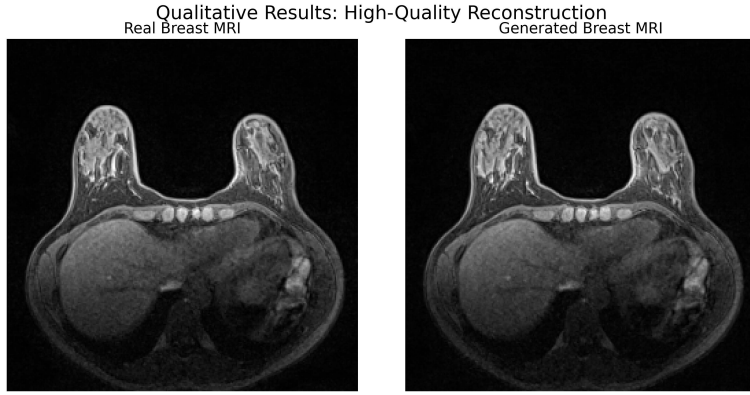


Fig. 2: Comparison of real and synthetic breast MRI images generated with Diffusion Model maintaining high fidelity and anatomical consistency.

3.2 Experimental Setup

Our experimental setup consists of two NVIDIA GeForce RTX 2070 graphics processing units, each equipped with 8GB of memory. The system runs on the Ubuntu Linux operating system, providing a stable and efficient computing environment for deep learning experiments. All experiments are conducted within a virtual environment to ensure reproducibility and isolate dependencies.

Model training is performed using batch processing to optimize memory utilization of both GPUs. The virtual environment is configured with specific package versions to ensure the compatibility and reproducibility of the results. All hyperparameters are carefully tuned based on preliminary validation experiments to achieve optimal performance while maintaining computational efficiency.

Specifically, our model configuration was tailored to the constraints of our low-data medical imaging task. We set the generated image resolution to 256x256 pixels, which maintains a balance between capturing sufficient anatomical detail for breast MRI analysis and maintaining computational feasibility. The model was trained for 200 epochs to ensure adequate learning without overfitting. Employed a relatively low learning rate of 2e-5, which has been empirically validated to provide stable training dynamics for diffusion models.

3.3 Denoising Trajectory and Explainability Observation

To analyze the internal behavior of the trained diffusion model, we performed a stepwise visualization of the denoising process using our own model. The main objective was to understand how the model reconstructs anatomical structures from pure noise over multiple diffusion timesteps and to observe the gradual emergence of meaningful visual features.

The experiment began with a randomly initialized noise image concatenated with a binary segmentation mask representing the breast region. At the initial

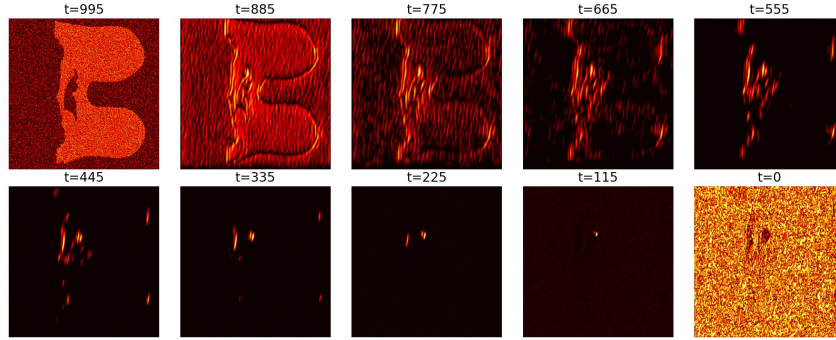


Fig. 3: Visualization of the denoising trajectory across diffusion timesteps. Each frame represents the predicted noise magnitude at a specific stage of the generative process. The progression demonstrates how the trained diffusion model gradually reconstructs the anatomical features of breast MRI images through iterative denoising.

step, the input consisted of pure Gaussian noise with no discernible structure. As denoising progressed, the model iteratively refined the noise distribution, with anatomical outlines and intensity patterns gradually emerging. By the final timestep ($t = 995$), the generated image displayed a coherent breast MRI structure consistent with real images from the dataset. To interpret this process, we examined the noise prediction maps at each stage, representing the magnitude and spatial distribution of estimated noise. Early stages showed diffuse, high-intensity noise, while later stages revealed localized suppression along tissue boundaries and glandular regions. This progressive reduction in noise magnitude illustrates how the model focuses on anatomically relevant areas, transforming unstructured noise into realistic medical imagery (Figure 3). These results demonstrate that the denoising process itself offers a clear form of explainability, where each diffusion step visibly transitions from random noise to meaningful anatomical structure.

3.4 Quantitative Analysis and Prototype Explainability

To evaluate the interpretability and quantitative performance of the trained diffusion model, three prototype based explainability architectures PPNet, EPP-Net, and ProtoPool, were applied to the generated breast MRI images. These models were used to compute Normalized Influence Scores (NIS) at Figure 5, which indicate how strongly each prototype from the training data contributes to the generation of a specific synthetic image. The faithfulness score derived from these influence distributions provides a quantitative measure of how accurately the prototype based explanations align with the actual generative process. Quantitative evaluation of our generated breast MRI images is provided in Table 1

Table 1: Quantitative evaluation of generated breast MRI images using standard image quality metrics.

Metric	Mean	SD	Observation
PSNR	19.37 ± 1.67		Stable pixel fidelity
SSIM	0.6530 ± 0.1052		Good structural match
LPIPS	0.2893 ± 0.1050		Strong perceptual quality

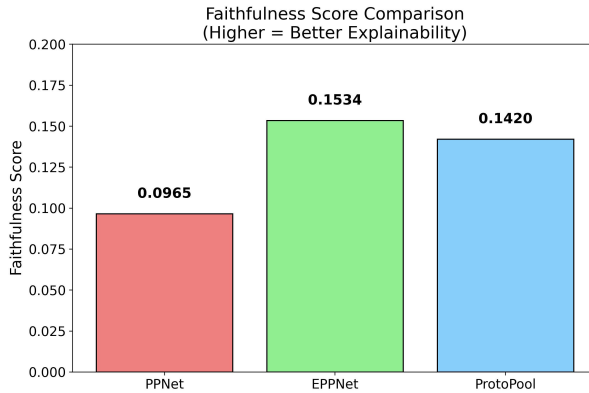


Fig. 4: Comparison of faithfulness scores among PPNet, EPPNet, and ProtoPool on synthetic breast MRI images. The bar chart highlights that EPPNet achieved the highest faithfulness score, indicating stronger alignment between prototype activations and the underlying diffusion generation process.

Across all models, the generated breast MRI images exhibited consistent visual quality, supported by high quantitative metrics. The diffusion model achieved a Peak Signal-to-Noise Ratio (PSNR) of 19.37 ± 1.67 , a Structural Similarity Index (SSIM) of 0.6530 ± 0.1052 , and a Learned Perceptual Image Patch Similarity (LPIPS) of 0.2893 ± 0.1050 . These results confirm that the generated images maintain both high fidelity and perceptual realism relative to the real dataset.

Regarding explainability, the comparative faithfulness analysis showed that EPPNet achieved the highest score of 0.1534, followed by ProtoPool with 0.1420, and PPNet with 0.0965. The superior performance of EPPNet reflects its enhanced prototype normalization and diversity constraints, which allow it to provide more reliable and interpretable associations between real and synthetic image regions Figure 4. ProtoPool also demonstrated strong generalization by dynamically reusing prototypes across structurally similar features, while PPNet, although simpler, produced more localized but less comprehensive explanations.

Overall, the results demonstrate that the proposed diffusion-based framework not only produces high-fidelity synthetic breast MRI images but also provides faithful and transparent explanations of the generative process. This combination

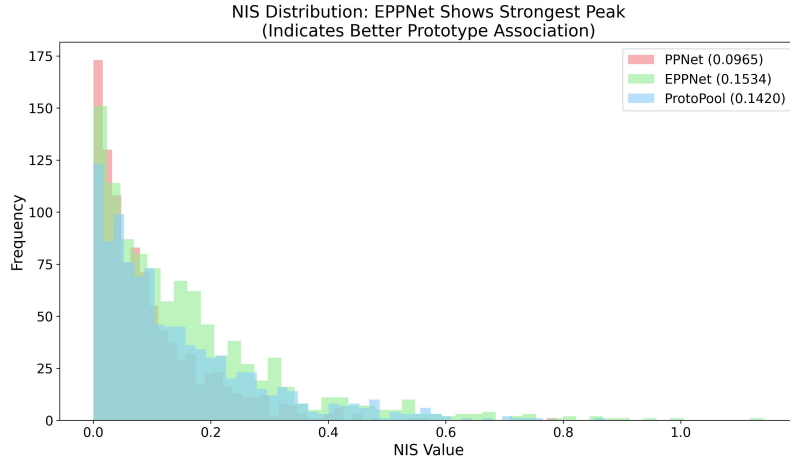


Fig. 5: Distribution of Normalized Influence Scores (NIS) across generated samples. The plot illustrates how prototype activations vary among PPNet, EPPNet, and ProtoPool, showing that EPPNet maintains the most balanced and distinct influence distribution across prototypes.

of visual quality and explainability marks a promising step toward trustworthy generative modeling in medical imaging.

3.5 Discussion

The overall findings of this study highlight the strength of diffusion models in generating realistic and interpretable medical images. The gradual denoising trajectory clearly shows how meaningful anatomical information emerges from pure noise, providing a visual understanding of the generative behavior of the model. This observation supports the idea that explainability can be naturally studied through the internal dynamics of diffusion processes, rather than relying solely on post hoc interpretation methods.

Quantitative results confirm that the proposed model achieves a strong balance between image quality and interpretability. The PSNR, SSIM, and LPIPS values indicate that the generated images maintain both pixel level and perceptual similarity with the real MRI data. Among the prototype based models, EPPNet produced the most consistent and faithful explanations, suggesting that prototype normalization and diversity regularization improve interpretability in single class medical imaging tasks. ProtoPool also demonstrated competitive performance, showing that flexible prototype sharing can generalize well across subtle variations in anatomical patterns.

These results emphasize that explainability and fidelity are not competing goals but complementary aspects of trustworthy generative modeling. By analyzing prototype contributions to image formation and the evolving denoising process, we gain clearer insight into the reasoning behind synthetic image

generation. This blend of transparency and realism offers a promising path for integrating generative AI into medical research and diagnostic support systems.

4 Conclusion

This study showed that diffusion models can generate realistic and anatomically accurate breast MRI images while also being explainable. By combining the diffusion process with prototype based methods like PPNet, EPPNet, and ProtoPool, we were able to understand how the model forms images and what parts of the training data influence them. The results suggest that EPPNet provides the most faithful explanations, proving that diffusion models can be both powerful and transparent. This work takes an important step toward building trustworthy systems for medical imaging.

Future work can extend this approach to multiclass tasks and multiple imaging modalities, including MRI and CT scans. The idea is to test how well the explainability holds when the model deals with more diverse data and to uncover any limitations that appear at scale. This will help us build a more stable, generalizable, and clinically useful explainable diffusion framework for medical imaging.

REFERENCES

- [1] Bhushan Atote and Victor Sanchez. Enhanced prototypical part network (eppnet) for explainable image classification via prototypes, 2024.
- [2] Bhushan Atote and Victor Sanchez. How were you created? explaining synthetic face images generated by diffusion models. In *European Conference on Computer Vision*, pages 263–278. Springer, 2024.
- [3] Chaofan Chen, Oscar Li, Daniel Tao, Alina Barnett, Cynthia Rudin, and Jonathan K Su. This looks like that: deep learning for interpretable image recognition. *Advances in neural information processing systems*, 32, 2019.
- [4] Zolnamar Dorjsembe, Hsing-Kuo Pao, Sodtavilan Odonchimed, and Furen Xiao. Conditional diffusion models for semantic 3d brain mri synthesis. *IEEE Journal of Biomedical and Health Informatics*, 28(7):4084–4093, 2024.
- [5] Ian J Goodfellow, Jean Pouget-Abadie, Mehdi Mirza, Bing Xu, David Warde-Farley, Sherjil Ozair, Aaron Courville, and Yoshua Bengio. Generative adversarial nets. *Advances in neural information processing systems*, 27, 2014.
- [6] Martin Heusel, Hubert Ramsauer, Thomas Unterthiner, Bernhard Nessler, and Sepp Hochreiter. Gans trained by a two time-scale update rule converge to a local nash equilibrium. *Advances in neural information processing systems*, 30, 2017.
- [7] Jonathan Ho, Ajay Jain, and Pieter Abbeel. Denoising diffusion probabilistic models. *Advances in neural information processing systems*, 33:6840–6851, 2020.
- [8] Jonathan Ho and Tim Salimans. Classifier-free diffusion guidance, 2022.
- [9] Anil K Jain. Fundamentals of digital image processing. 1989.
- [10] Lan Jiang, Ye Mao, Xiangfeng Wang, Xi Chen, and Chao Li. Cola-diff: Conditional latent diffusion model for multi-modal mri synthesis. In *International Conference on Medical Image Computing and Computer-Assisted Intervention*, pages 398–408. Springer, 2023.
- [11] Joanna Kaleta, Paweł Skierś, Jan Dubiński, Przemysław Korzeniowski, and Kamil Deja. Mediffusion: Joint diffusion for self-explainable semi-supervised classification and medical image generation. *arXiv preprint arXiv:2411.09434*, 2024.
- [12] Amirhossein Kazerouni, Ehsan Khodapanah Aghdam, Moein Heidari, Reza Azad, Mohsen Fayyaz, Ilker Hacihaliloglu, and Dorit Merhof. Diffusion models in medical imaging: A comprehensive survey. *Medical image analysis*, 88:102846, 2023.
- [13] Diederik P Kingma and Max Welling. Auto-encoding variational bayes. *arXiv preprint arXiv:1312.6114*, 2013.
- [14] Robin Rombach, Andreas Blattmann, Dominik Lorenz, Patrick Esser, and Björn Ommer. High-resolution image synthesis with latent diffusion models, 2022.
- [15] Dawid Rymarczyk, Lukasz Struski, Michał Górszczak, Koryna Lewandowska, Jacek Tabor, and Bartosz Zieliński. Interpretable image classification with differentiable prototypes assignment, 2022.
- [16] Ashirbani Saha, Michael R Harowicz, Lars J Grimm, Connie E Kim, Sujata V Ghate, Ruth Walsh, and Maciej A Mazurowski. A machine learning approach to radiogenomics of breast cancer: a study of 922 subjects and 529 dce-mri features. *British journal of cancer*, 119(4):508–516, 2018.
- [17] Ammar A Siddiqui, Santosh Tirunagari, Tehseen Zia, and David Windridge. Vald-md: visual attribution via latent diffusion for medical diagnostics. *arXiv preprint arXiv:2401.01414*, 2024.

- [18] Ammar Adeel Siddiqui, Santosh Tirunagari, Tehseen Zia, and David Windridge. A latent diffusion approach to visual attribution in medical imaging. *Scientific Reports*, 15(1):962, 2025.
- [19] Yang Song, Jascha Sohl-Dickstein, Diederik P. Kingma, Abhishek Kumar, Stefano Ermon, and Ben Poole. Score-based generative modeling through stochastic differential equations, 2021.
- [20] Zhou Wang, Alan C Bovik, Hamid R Sheikh, and Eero P Simoncelli. Image quality assessment: from error visibility to structural similarity. *IEEE transactions on image processing*, 13(4):600–612, 2004.
- [21] Richard Zhang, Phillip Isola, Alexei A Efros, Eli Shechtman, and Oliver Wang. The unreasonable effectiveness of deep features as a perceptual metric. In *Proceedings of the IEEE conference on computer vision and pattern recognition*, pages 586–595, 2018.